01 Feb 2014

Modeling the Construction of Polymeric Adsorbent Media: Effects of Counter-Ions on Ligand Immobilization and Pore Structure

Enrico Riccardi

Jee-Ching Wang
Missouri University of Science and Technology, jcwang@mst.edu

Athanasios I. Liapis
Missouri University of Science and Technology, ail@mst.edu

Recommended Citation

E. Riccardi et al., "Modeling the Construction of Polymeric Adsorbent Media: Effects of Counter-Ions on Ligand Immobilization and Pore Structure," *Journal of Chemical Physics*, vol. 140, no. 8, American Institute of Physics (AIP), Feb 2014.
The definitive version is available at https://doi.org/10.1063/1.4865910

Modeling the construction of polymeric adsorbent media: Effects of counter-ions on ligand immobilization and pore structure

Enrico Riccardi, Jee-Ching Wang, and Athanasios I. Liapis

Citation: The Journal of Chemical Physics **140**, 084901 (2014); doi: 10.1063/1.4865910
View online: https://doi.org/10.1063/1.4865910
View Table of Contents: http://aip.scitation.org/toc/jcp/140/8
Published by the American Institute of Physics

Modeling the construction of polymeric adsorbent media: Effects of counter-ions on ligand immobilization and pore structure

Enrico Riccardi,[1] Jee-Ching Wang,[2] and Athanasios I. Liapis[2,a)]
[1]*Ugelstad Laboratory, Department of Chemical Engineering, Norwegian University of Science and Technology, Sem Saelands vei 4, NO-7491 Trondheim, Norway*
[2]*Department of Chemical and Biochemical Engineering, Missouri University of Science and Technology, 400 West 11th Street, Rolla, Missouri 65409-1230, USA*

(Received 30 December 2013; accepted 4 February 2014; published online 24 February 2014)

Molecular dynamics modeling and simulations are employed to study the effects of counter-ions on the dynamic spatial density distribution and total loading of immobilized ligands as well as on the pore structure of the resultant ion exchange chromatography adsorbent media. The results show that the porous adsorbent media formed by polymeric chain molecules involve transport mechanisms and steric resistances which cause the charged ligands and counter-ions not to follow stoichiometric distributions so that (i) a gradient in the local nonelectroneutrality occurs, (ii) non-uniform spatial density distributions of immobilized ligands and counter-ions are formed, and (iii) clouds of counter-ions outside the porous structure could be formed. The magnitude of these counter-ion effects depends on several characteristics associated with the size, structure, and valence of the counter-ions. Small spherical counter-ions with large valence encounter the least resistance to enter a porous structure and their effects result in the formation of small gradients in the local nonelectroneutrality, higher ligand loadings, and more uniform spatial density distributions of immobilized ligands, while the formation of exterior counter-ion clouds by these types of counter-ions is minimized. Counter-ions with lower valence charges, significantly larger sizes, and elongated shapes, encounter substantially greater steric resistances in entering a porous structure and lead to the formation of larger gradients in the local nonelectroneutrality, lower ligand loadings, and less uniform spatial density distributions of immobilized ligands, as well as substantial in size exterior counter-ion clouds. The effects of lower counter-ion valence on pore structure, local nonelectroneutrality, spatial ligand density distribution, and exterior counter-ion cloud formation are further enhanced by the increased size and structure of the counter-ion. Thus, the design, construction, and functionality of polymeric porous adsorbent media will significantly depend, for a given desirable ligand to be immobilized and represent the adsorption active sites, on the type of counter-ion that is used during the ligand immobilization process. Therefore, the molecular dynamics modeling and simulation approach presented in this work could contribute positively by representing an engineering science methodology to the design and construction of polymeric porous adsorbent media which could provide high intraparticle mass transfer and adsorption rates for the adsorbate biomolecules of interest which are desired to be separated by an adsorption process. © *2014 AIP Publishing LLC*. [http://dx.doi.org/10.1063/1.4865910]

I. INTRODUCTION

Recent advances in molecular biology and separation science have contributed significantly to the large-scale production of diagnostics and biotherapeutics. In the downstream purification and separation processes involved in the production of bioactive molecules, a large sequence of steps is typically required and ion exchange chromatography (IEC) represents a major adsorption-separation method for this purpose.[1–5] In order to increase the adsorptive capacity while maintaining efficient mass transfer rates, the pore surface of the base porous matrix of the IEC porous adsorbent particle (e.g., agarose) is most often grafted with polymeric extender molecules that form a porous layer on the surface of the base matrix, and then functionalized by immobilizing desirable ligands onto the porous extender layer.[4–11] The coupling between the extender and the base matrix and between the ligands and the extender is desired to be strong and is achieved typically by covalent bonds. Depending on the charge type of the adsorbate biomolecules, the selected to be immobilized ligands are introduced together with counter-ions and can be either positively charged (e.g., ammine groups[6,7]) or negatively charged (e.g., carboxyl, sulfonic acid groups[6,8]). It is thus beneficial in the construction and utilization of IEC adsorbent media to regard the construction of the porous extender layer on a base matrix as Stage I,[9] immobilization of charged ligands onto the extender layer as Stage II,[4,5,10,11] and subsequent transport and adsorption (onto the immobilized ligands) of a charged adsorbate biomolecule in the resultant adsorbent medium as Stage III.[4,5] In addition to the more apparent dependencies on the loading and density distribution of the immobilized ligands, the performance of an IEC adsorption system has also been found to depend on the pore structure of the extender

a)Author to whom correspondence should be addressed. Electronic mail: ail@mst.edu. Telephone: +1-573-341-4414. Fax: +1-573-341-4377.

layer and the dynamics of the transport and adsorption mechanisms of the biomolecule.[3–5,9–23] In fact, these latter two factors can be directly affected[4,5,9–12,23] by the former two. It could thus be understood that through the mechanisms and processes taking place in Stages I, II, and III, many of the factors involved in the construction of an IEC adsorbent medium have direct or indirect effects on the dynamic and equilibrium performance of an IEC chromatography system.

During the immobilization process of charged ligands, counter-ions with charges opposite to that of the charged ligands but of the same type as that of the adsorbate biomolecule of interest are employed to maintain global electroneutrality for the adsorbent medium under construction. Due to their continuous interactions with other charged species in the system and their relatively high mobility, counter-ions could be expected to have additional effects, which, however, have traditionally been overlooked as most attention and effort have been devoted to the charged ligands and most molecular dynamics (MD) modeling and simulations studies as well as most studies employing macroscopic continuum models have not explicitly considered or have been negligent about the effects of the counter-ions. In our recent studies[4,5,10–12,21–23] where the counter-ions are treated more realistically as discrete charged species, the counter-ions have been shown to have significant effects on the immobilization process of the charged ligands, the pore structure of the polymeric extender layers, and the transport and adsorption of adsorbate biomolecules. Furthermore, when counter-ions with the same spherical shape and diameter but different $+1e$ or $+2e$ charges are employed in the same ligand immobilization process carried out in an MD modeling and simulation study, they were found to result in significantly different spatial distributions of counter-ions and immobilized ligands as well as pore size distributions and pore connectivities in the resultant porous polymeric extender layers.[23] In addition, counter-ions in other systems containing assemblies of chain molecules immersed in electrolytic solutions[24–29] have also been observed to play significant roles in determining the properties and dynamic behavior of the examined systems. These findings together support the thesis that the effects of counter-ions should be considered to be very important during the construction and utilization of IEC adsorbent media. They further suggest that it is plausible to utilize different types of counter-ions as a means to control the process of ligand immobilization and the pore structure of the extender layer so that the constructed adsorbent media could provide desirable distributions of ligand density, pore size, and pore connectivity[4,5,10,11] in order to fulfill different needs of use in IEC adsorption systems.

Our recent MD study[23] that considered and compared the ligand immobilization processes with singly and doubly charged counter-ions can be considered to focus on the valence aspect of the effects of counter-ions on the IEC adsorption systems. Considering the strong Coulombic interactions between the charged ligands and counter-ions, coupled with the structural flexibility of and nanometer scale spacing (pore opening) between the polymeric extender molecules, the counter-ions could have additional complicated effects on the construction and utilization of the IEC polymeric adsorbent media, which could make the traditional framework in terms of enthalpic and entropic effects for analyzing complex systems inadequate. This work is intended to uncover additional aspects of the counter-ion effects by employing counter-ions with different numbers and distributions of charges and with different structures for the same ligand immobilization process. In a broader context of engineering science, the findings from this work could have important implications to other relevant systems containing charged solutes and assemblies of chain molecules.

II. MOLECULAR DYNAMICS MODELS AND SIMULATION METHODS

The MD modeling and simulation approach employed in this work is based on a set of satisfactory coarse-grain models which have been successfully implemented in the computational design and construction of polymeric porous adsorbent media.[9–11,23] It is important to mention here that the results obtained from atomistic modeling and simulations employed in the construction of polymeric porous adsorbent media[4,30] are satisfactorily represented by the results determined from the coarse-grain models employed in this work.

In order to facilitate comparison and analysis on a consistent basis, the simulations of the immobilization process (Stage II) taking place in the presence of the different counter-ions considered in this work, employ the same initial condition which is represented by the same porous dextran layer which is obtained at the end of the grafting process of dextran polymer chains onto the porous base matrix of agarose (Stage I). Since the details of the system formulation and simulation models have been described in Refs. 9–11, 23, 31, only a brief summary is given here. The base matrix is represented by a non-flat agarose surface whose interaction with any other species i located at (x,y,z) is treated by the following model:[9–11,23]

$$U_{is}(x,y,z) = 2\pi\varepsilon_{is}\left(\frac{\sigma_{is}}{R_{0s}}\right)^2, \times\left[\frac{2}{5}\left(\frac{\sigma_{is}}{z_s}\right)^{10} - \left(\frac{\sigma_{is}}{z_s}\right)^4 - \frac{\sqrt{2}}{3\left(\frac{R_{0s}}{\sigma_{is}}\right)\left(\frac{z_s}{\sigma_{is}} + \frac{0.61}{\sqrt{2}}\frac{R_{0s}}{\sigma_{is}}\right)^3}\right], \tag{1a}$$

$$z_s = z - a\left[2 + \cos\left(\frac{2\pi}{b}x\right) + \cos\left(\frac{2\pi}{b}y\right)\right], \tag{1b}$$

where $\sigma_{is} = (\sigma_i + R_{0s})/2$, $\varepsilon_{is} = \sqrt{\varepsilon_i\varepsilon_{0s}}$, σ_i, and ε_i are the size and interaction parameters of the particle, and R_{0s} and ε_{0s} represent the nearest distance and interaction strength, respectively, between the pseudomonomers that constitute the model surface. As indicated by Eq. (1b), the non-flat surface features sinusoidal corrugations whose amplitude and wavelength are governed by the values of the a and b parameters,[9] respectively. Twenty dextran chains, each having 40 glucose monomers per main chain, a monomeric side branch, and

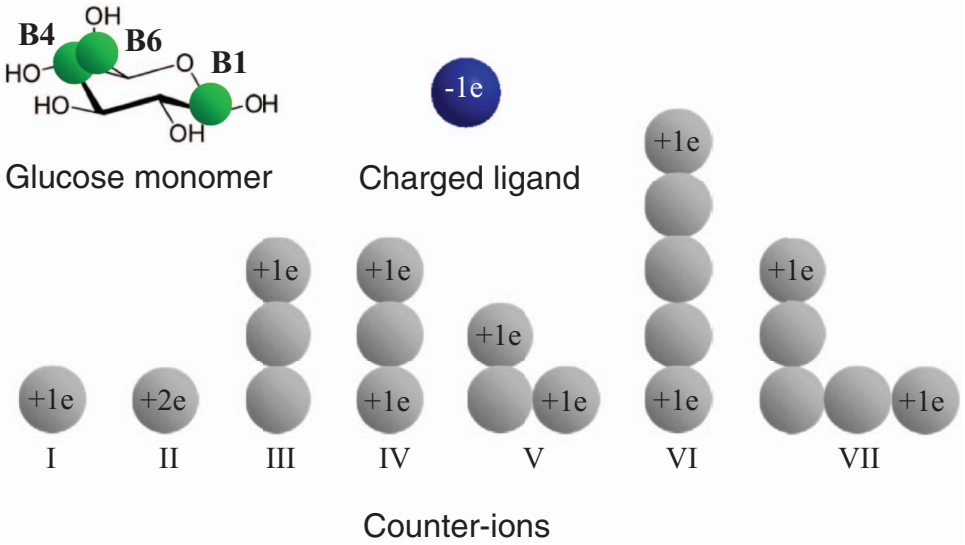

FIG. 1. Coarse-grain bead models and color representations of the M3B glucose monomer, the charged ligand, and the seven different types of counter-ions employed in this work.

a dimeric side branch (5% of side branching), are grafted at randomly selected locations on the non-flat agarose surface. The dextran chains are simulated with a modified M3B model where each glucose monomer is represented by three beads located at the positions of C1, C4, and C6 carbon atoms and denoted as B1, B4, and B6.[9–11,23,31] Between the M3B beads, the bond lengths are constrained by the SHAKE algorithm[32] and the bending and torsional motions[9–11,23,30–32] are treated by the rather standard $U_{\text{bend}}(\theta) = \frac{1}{2}K_\theta(\theta - \theta_0)^2$ and $U_{\text{tor}}(\phi) = \sum_{j=1}^{3} \frac{1}{2}B_j[1 + \cos(j\phi - \phi_j^0)]$ models, respectively. The values of a, b, R_{0s}, ε_{0s}, K_θ, θ_0, B_j, and ϕ_j^0 used in this work are the same as in our previous studies.[9–11,23] The dextran chains are completely immersed in an isothermal-isobaric aqueous phase represented by coarse-grain water molecules within the same M3B model.[9–11,23,31] The aqueous phase extends in the perpendicular z direction (direction of net mass transport) to z = 130 Å and develops a water-vapor (vacuum) interface which is at least 50 Å above the top of the equilibrated dextran porous layers. The system along the lateral x and y directions has linear dimensions of 202 Å × 202 Å coupled with the usual implementation of periodic boundary conditions.

As considered in our previous study[23] and as shown in Figure 1, the ligands employed in this work carry –1e charge and have a spherical shape of 6.7 Å in diameter and a molecular weight of 75 g/mol. Seven different types of counter-ions, as depicted in Figure 1, are considered to take part in the ligand immobilization process and they are constructed with the same M3B beads that have a diameter of 4.7 Å and a molecular weight of 45 g/mol.[23,31] Between these M3B beads in the counter-ions, the bond lengths are constrained to 2.51 Å and the bond angles are maintained around either 0° or 90° by $U_{\text{bend}}(\theta) = \frac{1}{2}K_\theta(\theta - \theta_0)^2$ with k_θ = 100 kcal/mol-rad^2.[23,31] The selection of these model counter-ions could enable one to study (i) the effects of counter-ion length/size by comparing the results determined from counter-ions of types I and III and from types II, IV, and V, (ii) the effects of counter-ion geometric shape by comparing the results obtained from counter-ions of types IV and V and from types VI and VII, and (iii) simultaneously the mixed effects of counter-ion valence, size, and/or shape by comparing the results determined from all relevant cases. In addition to the Coulombic interactions between charges and the above conformational potential models, non-bonded van der Waals interactions are needed in order to represent other intrinsic interactions in the systems and prevent physically implausible overlaps between oppositely charged beads. Such non-bonded interactions among the M3B beads in dextran chains, ligands, and counter-ions and those between the water molecules and the M3B beads are described by Morse potentials with appropriately different parameter values that have also been employed in previous studies.[9–11,23,31]

The MD simulations in this work are carried out using the leap frog integration algorithm[32] and a Gaussian thermostat method[32,33] to control the temperature at 300 K. The base dextran porous structure is equilibrated in water first before the ligands are immobilized. Following our previous MD studies,[10,11,23] the process of ligand immobilization proceeds in a stepwise manner and starts first with 50 ligands and a corresponding number of counter-ions matched for global electroneutrality. The ligands and the counter-ions are randomly placed in the bulk-like aqueous phase above the dextran layer and are given velocities sampled from the equilibrium velocity distributions at the system temperature with perpendicular components always pointing towards the dextran layer. Once a ligand molecule moves within a certain qualified distance[10,11,23] from a vacant B4 site in the dextran layer, it is considered covalently immobilized and its distance to the B4 site is constrained by SHAKE[32] to the B1–B4 bond length until the end of the simulation. After one or two ligands are immobilized depending on the valence and loading of the counter-ions, new ligands and counter-ions are introduced into the bulk-like aqueous phase above the dextran layer by the same sampling approach to maintain the same

number of unattached ligands and the immobilization driving force in the system. For a balance between computational efficiency and a realistic representation of the actual process, the ligand immobilization process is halted and the simulation system is relaxed and re-equilibrated[10,11,23] when the number of immobilized ligands reaches multiples of 50. However, this halting and re-equilibration procedure needs to be used more frequently for increasingly smaller increments of immobilized ligands when the ligand immobilization process encounters increased difficulty toward the maximum loading. In order to be considered equilibrated and provide realistic representations of the IEC adsorbent media at the end of Stage II for further analysis in this work, all systems are required to pass two criteria: (a) the immobilization process proceeds beyond a minimum loading of 0.5 ligands per B4 site and the immobilization rate decreases with time and (b) no more than one new ligand is immobilized in the last 3 ns of the simulated immobilization process.

After equilibration, the pore structures are visually examined by simulation snapshots and quantitatively characterized in terms of the distributions of the number of pore openings and pore radii by dividing a model system into two levels of cubic lattices at the angstrom level[23,34] and at each lattice point concentric disks of varying diameters but of the same thickness of choice, namely, 3.77 Å which is the diameter of a coarse-grain water molecule, are utilized to probe local openings formed by the dextran beads and the immobilized ligands which are covalently bonded and permanent parts of the porous layers. The level of pore connectivity[23,34] can then be ascertained by the extent of intersection between different distribution curves that represent pores of different size ranges as well as by visual examination of simulation snapshots of different cross sections of the resultant dextran layers.

III. RESULTS AND DISCUSSION

Starting initially with the same base dextran porous layer and with the same ligand and immobilization procedure,[23] the dextran chains and the pore structure respond relatively similarly to the first batches of ligands and the seven different employed counter-ions because the pores are still very open and the numbers of the charged ligands and counter-ions are still low. As the number of batches of ligands and counter-ions increase, the use of the different counter-ions imposes different effects on the porous structure, as can be seen in Figure 2 where the simulation snapshots of the seven

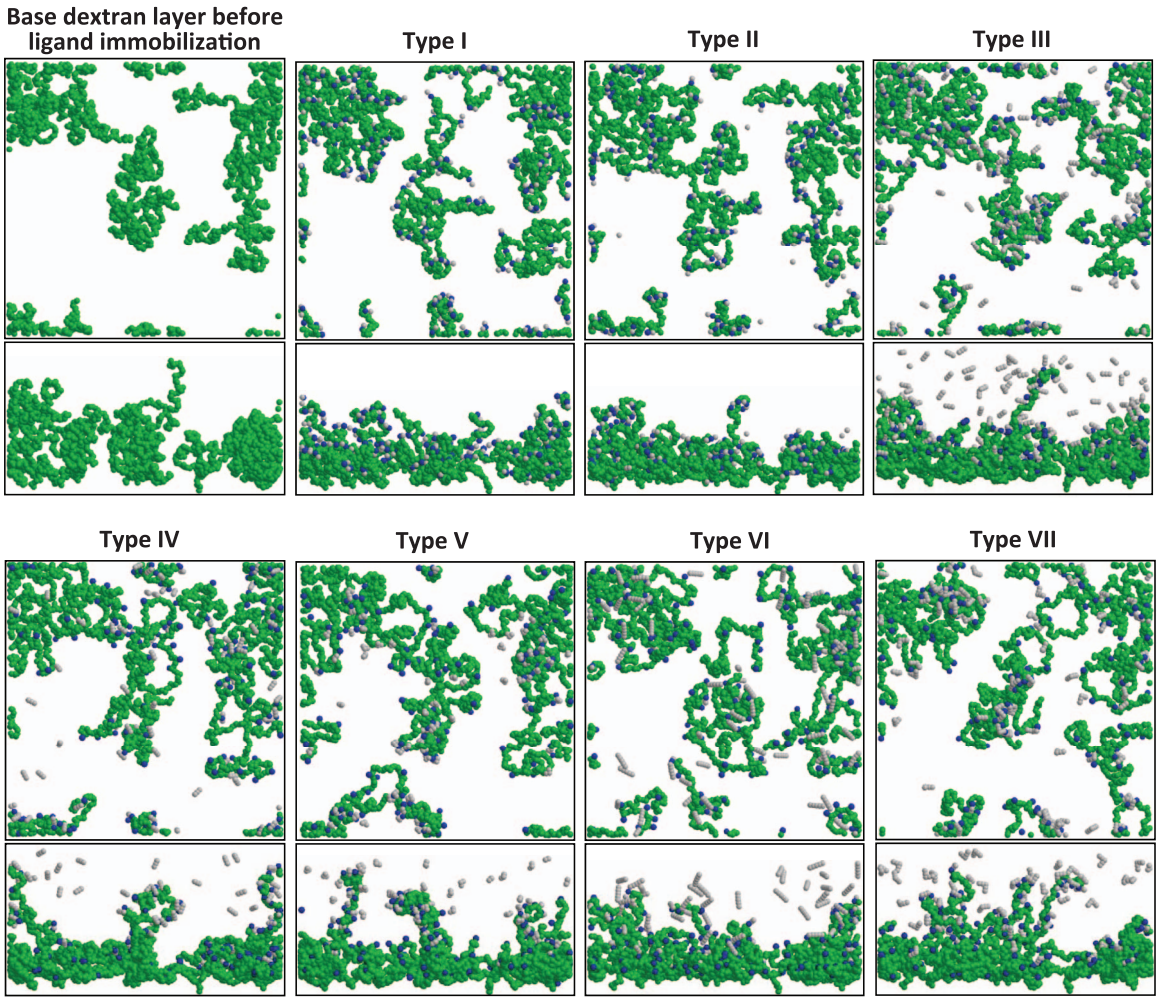

FIG. 2. yx top-down views and yz side views of the dextran (green beads) porous layers with 150 immobilized charged ligand molecules (blue beads) and seven different types of counter-ions (gray beads). For visual clarity, water molecules are not shown.

different counter-ion cases with 150 immobilized ligands for each case are presented along with those of the base dextran porous layer for comparison. Under this relatively low ligand loading, although the lateral configurations of the initial pore structure could still be considered to be retained to some extent based on the resemblance of their top-down views in Figure 2, the seven different counter-ion cases already exhibit different effects and steer the ligand immobilization process and the porous layer towards different evolution paths, as indicated clearly by the side views in Figure 2. While counter-ions of types I and II, which have the smallest size and simplest geometric shape, can still be easily accommodated by the porous layer and consequently leave no counter-ions outside the dextran layer and give rise to higher levels of thickness compaction, the other types of counter-ions employed already start to have difficulty to be incorporated into the dextran layer. Interestingly, these exterior counter-ions which remain outside the dextran layer and are dispersed in the aqueous fluid phase appear to equip the systems with interphase Coulombic interactions that help stabilize stretched conformations of dextran chains, thereby causing the dextran layers to present more corrugated interfaces to the bulk fluid and incoming species. In addition, these exterior counter-ions also cause the dextran layers to have non-zero net charges and internal charge-charge repulsions that, as demonstrated by the top-down views in Figure 2, also make the pore structures more fractured laterally.

In addition to the differences in the dynamics of ligand immobilization discussed above, the seven different counter-ions employed also allow different numbers of charged ligands to be immobilized in the equilibrated systems. The results are summarized in Table I and show that the highest numbers of immobilized ligands are obtained with counter-ions of types I and II, followed by those of types V, IV, and VII, and significantly lower numbers of immobilized ligands are obtained when counter-ions of types III and VI are used. These equilibrium ligand loading numbers vary about ∼30% and clearly indicate the significant effects on ligand immobilization of the different counter-ions due to their charges, sizes, and shapes. It is important and beneficial to examine at this point the differences in the mechanisms of ligand immobilization and counter-ion incorporation into the porous dextran layer. The immobilization of ligand is driven by the formation of covalent bonds with the B4 beads of the dextran chains, which is direct and permanent, while the incorporation of counter-ions is driven by their Coulombic interactions with the oppositely charged ligands that have bonded previously on the dextran chains, which is non-permanent and contingent on the number of immobilized ligands. However, without the incorporation of counter-ions, the immobilized charged ligands could cause the dextran chains to repel each other and develop an electrical resistance against subsequent ligand immobilization. This mechanistic interplay can be further complicated by the structural flexibility and steric hindrance of the dextran chains.[9–11,23] To illustrate these effects more explicitly, the simulation snapshots of the top-down and side views of the base dextran porous layer and the seven different equilibrated porous media after ligand immobilization are shown in Figure 3.

TABLE I. Numbers of immobilized ligands and their corresponding ligand loadings per B4 site in the presence of seven different types of counter-ions.

Counter-ion type	I	II	III	IV	V	VI	VII
Number of immobilized ligands at equilibrium	636	617	446	573	597	443	535
Equilibrium ligand loading per B4 site	0.74	0.72	0.52	0.67	0.69	0.52	0.62

Previous MD studies[9–11,23] and the dynamics of ligand immobilization discussed above have shown that the immobilized charged ligands and the incorporated counter-ions increase the cohesive energy and reduce the thickness of the dextran porous layer through their Coulombic interactions. These tendencies can also be observed in Figure 3 where the seven different types of employed counter-ion systems are presented and reach higher levels under maximum ligand loadings. Types I and II counter-ion systems continue with their dynamic behavior as observed during ligand immobilization and have significantly fewer exterior counter-ions being kept above the dextran porous layers, while other types of counter-ions encounter substantially greater difficulty to enter the porous structures and consequently have larger portions of their molecules remaining outside the dextran layers forming exterior clouds of counter-ions above the dextran layers. Such difficulty in general can be ascribed as due to steric resistances because it is associated with the relatively large sizes and non-compact shapes of the counter-ions and also partly rooted in the relatively narrow pore sizes and limited structural flexibility of the dextran chains. The counter-ion length/size effect can be more directly confirmed by the comparisons of the side views and the numbers of immobilized ligands between types I and III counter-ions, both carrying $+1e$ charges, and between types II, IV, and VI counter-ions, all three carrying $+2e$ charges. Similar comparisons between types IV and V and between types VI and VII counter-ions can also reveal an effect of counter-ion geometric shape such that the counter-ions with more compact shapes (types V and VII) lead to more ligands being immobilized and fewer counter-ions being kept outside the dextran layers than those resulting from their elongated counterparts carrying the same number of charges. These observations clearly indicate the inadequacy of neglecting the discrete sizes of ions in the modeling involved in studies examining the behavior of relevant systems. In fact, counter-ions have also been found to exert size effects on the formation of surfactant aggregates[24–27] and on the transport of species through membranes.[28] The effects of counter-ion valence can also be studied by comparing the results of types III and IV counter-ions where the type III counter-ion with a weaker valence leads to a smaller level of ligand loading and less compact porous structure. Interestingly, the differences between the results of types III and IV counter-ions are much greater than those between the results of types I and II counter-ions whose valences also differ by +1e. These findings together explain the observation that the type III counter-ion is the weakest among those studied in assisting ligand immobilization and in compacting the thickness of the dextran layer, and further suggest that the structure, primarily the length/size

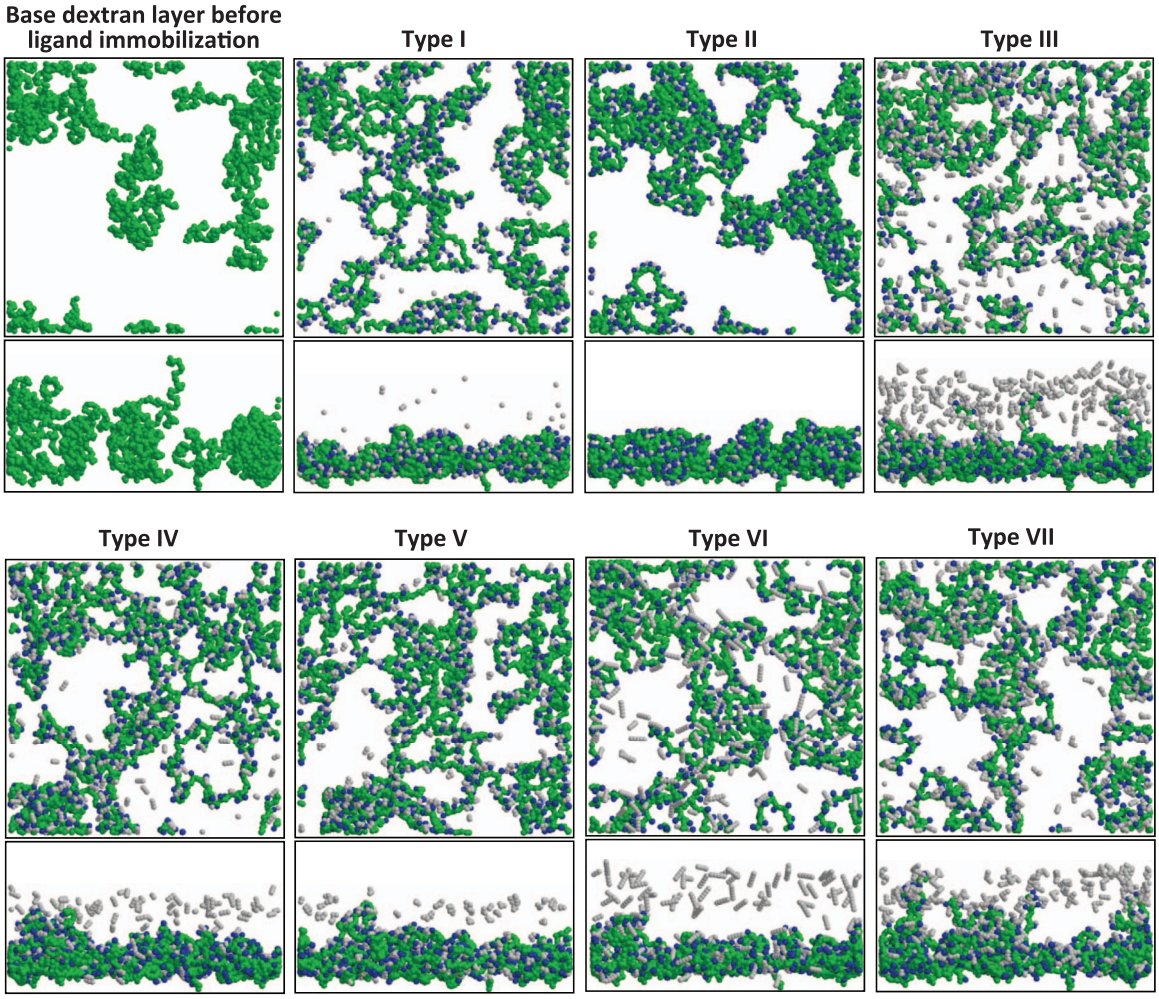

FIG. 3. yx top-down views and yz side views of the equilibrated dextran (green beads) porous layers with the charged ligands (blue beads) and seven different types of counter-ions (gray beads). For visual clarity, water molecules are not shown.

and also the shape, of a counter-ion is a very significant factor in determining the outcome of ligand immobilization during Stage II in the construction of IEC porous adsorbent media. This structural factor, which could be categorized as an entropic factor from a classical perspective, it will also naturally have very important implications to the mass transport and adsorption rates of the adsorbate biomolecules during Stage III where the polymeric porous adsorbent media are employed in chromatographic separations.[4]

For a more quantitative analysis, the spatial density distributions of the charged ligands, counter-ions, and net charges along the net mass transport direction, z, from the valleys of the non-flat surface are calculated using cross-sectional slices of 3.77 Å (coarse-grain water molecular diameter) in thickness. The results are presented in Figure 4, where many regions in the seven different porous dextran layers have ligand number densities exceeding the density of B4 sites in the "bulk-like" region of the base dextran layer (0.44 nm^{-3}),[23] and serve to indicate the compaction of the dextran layer structure and the reduction of its thickness. In addition, the absence and presence of the exterior counter-ion clouds discussed above can be easily seen in Figure 4. For further analysis, it is important and beneficial to first note that global electroneutrality is maintained in all the simulated systems employing different counter-ions at every time instant during each ligand immobilization process. However, the porous adsorbent systems have intrinsic features due to different mechanisms and steric resistance for the ligands and counter-ions to enter the porous layers as mentioned above that cause the charged ligands and the counter-ions not to follow stoichiometric distributions and consequently generate local nonelectroneutrality gradients and this represents a persistent phenomenon that can be observed in all the different cases studied in this work and shown in Figure 4. The results in Figures 3 and 4 indicate that the local nonelectroneutrality gradients as well as the formation of an exterior counter-ion cloud can be minimized when using the counter-ions with the least steric resistance (types I and II) to enter the porous layer and, thus, they possess the greatest capability in assisting ligand immobilization. In contrast, counter-ions bigger in size, more elongated in shape, and/or carrying smaller amounts of valence charges than those of types I and II, encounter significantly greater steric resistances to enter the porous layer and result in substantially larger local nonelectroneutrality gradients and large counter-ion clouds. For these reasons and consistent with the findings and discussion presented above, the

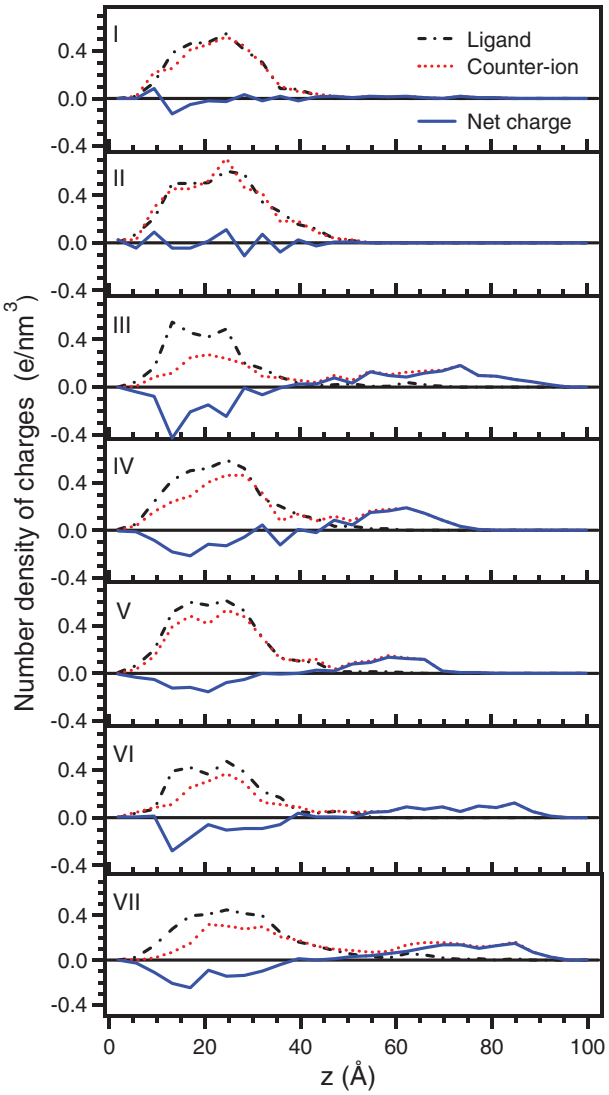

FIG. 4. Spatial number density distributions (e/nm^3) of the charged ligands, counter-ions, and net charges along the net mass transport direction, z, from the valleys of the non-flat surface.

counter-ion type III is the counter-ion that produces the largest gradient in local nonelectroneutrality and largest counter-ion cloud. Furthermore, the spatial density distributions of the immobilized ligands, which will serve as the adsorption sites for the adsorbate biomolecules during Stage III, can be seen to be mostly non-uniform, as observed and discussed before,[10,11,23] in particular those resulting from the two counter-ions of types III and VI which have the greatest difficulties to be incorporated into the porous dextran layer and provide the lowest levels of ligand immobilization and, furthermore, the immobilized ligands appear to exhibit bimodal distributions (in other words, bimodal distributions of adsorption sites). It is also worth mentioning here that the mechanisms of the porous layer underlying the formation of large exterior counter-ion clouds, large gradients in the local nonelectroneutrality, and non-uniform spatial density distributions of immobilized ligands are also those that cause steric resistance to counter-ions. These mechanisms and the resultant steric resistances presented by the porous layer are at play from the beginning of the ligand immobilization process and cause the formation of exterior counter-ion clouds to start being built early and continue to be developed throughout the duration of the ligand immobilization process as demonstrated by the results in Figures 2 and 3. The top-down views in Figures 2 and 3 also show that the dynamic and equilibrium spatial distributions of the exterior counter-ions are not random or uniform but correlate well with those of the immobilized ligands, indicating strong and specific interphase Coulombic interactions between the exterior counter-ion clouds and the dextran layers functionalized by the immobilized charged ligands. Based on these observations and the underlying fundamental mechanisms, the exterior counter-ion clouds as seen in this work, could be reasoned to be present and kinetically stable in the actual systems with similar features and mechanisms. Hypothetically, if the porous dextran layer is suddenly dissolved or very significantly altered so that its steric resistance becomes negligible, the counter-ions will quickly approach the charged ligands and the exterior counter-ion clouds and the gradient in the local nonelectroneutrality will be diminished. Since the adsorbate biomolecules of interest to be transported through the pore fluid of the porous polymeric adsorbent media and subsequently adsorbed onto the immobilized ligands carry the type of charge as that being carried by the counter-ions, the phenomenon of the formation of a counter-ion cloud adjacent to the adsorbent layers could be inferred to have profound and adverse effects on the mass transfer and adsorption rates of the adsorbate biomolecules.[4] More specifically, an exterior counter-ion cloud with a high spatial density above an adsorbent medium will present both spatial and electrical barriers which could potentially repel adsorbate biomolecules from entering the porous medium in operationally considered significant numbers. Under such a circumstance, minimizing the spatial density of the exterior counter-ion cloud can significantly improve the effective mass transfer and adsorption rates of adsorbate biomolecules. For this purpose, one could speculate that much like a "magnet" collecting scattered steel nails, polyelectrolytic species can be used to remove or reduce the formation of an exterior counter-ion cloud.

From previous analysis[23] and the snapshots shown in Figures 2 and 3, the base dextran layer can be seen to have a pore structure that has a small number of big pores and a significantly larger number of small pores. As revealed by the top-down views, a general effect of ligand immobilization, except perhaps when type II counter-ion is employed, is to make the pore structure more uniform laterally in terms of pore sizes and pore locations. In order to aid the analysis of the pore structures and compare them using the results from the ligand immobilization process where seven different counter-ions have been used, quantitative characterization of a porous structure can be accomplished by the procedure described above that maps the system into two levels of cubic lattices at an angstrom level.[9–11,23,34] The resultant spatial distributions of the pore openings of different sizes are summarized into different spatial distribution curves along the z axis of net mass transport and those resulting from the systems whose counter-ions form significant exterior counter-ion clouds, are presented in Figure 5. In general, the largest pores exist in the outer interfacial regions of the dextran layers where the

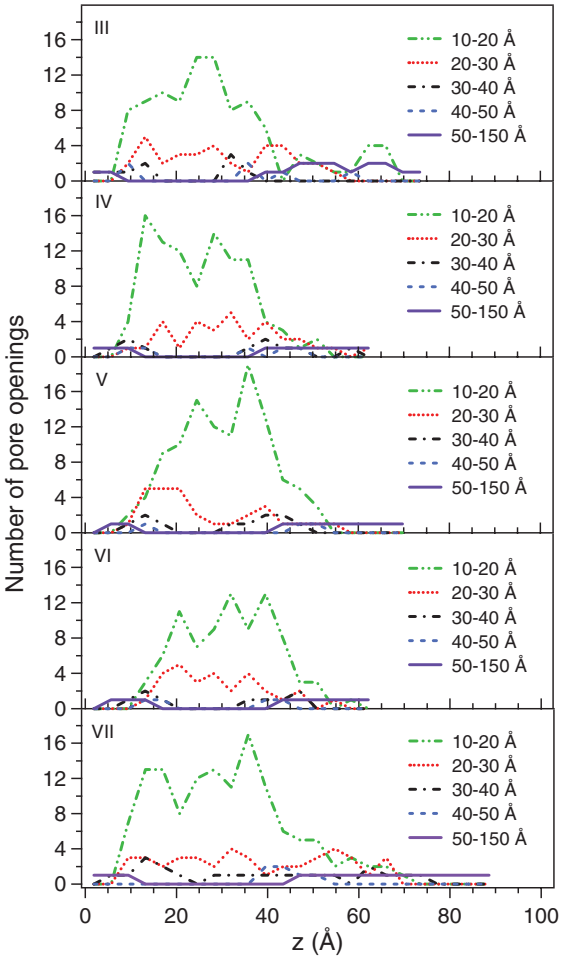

FIG. 5. Pore size distributions in the porous dextran layers resulting from the immobilization of ligands in systems employing counter-ions of types III, IV, V, VI, and VII.

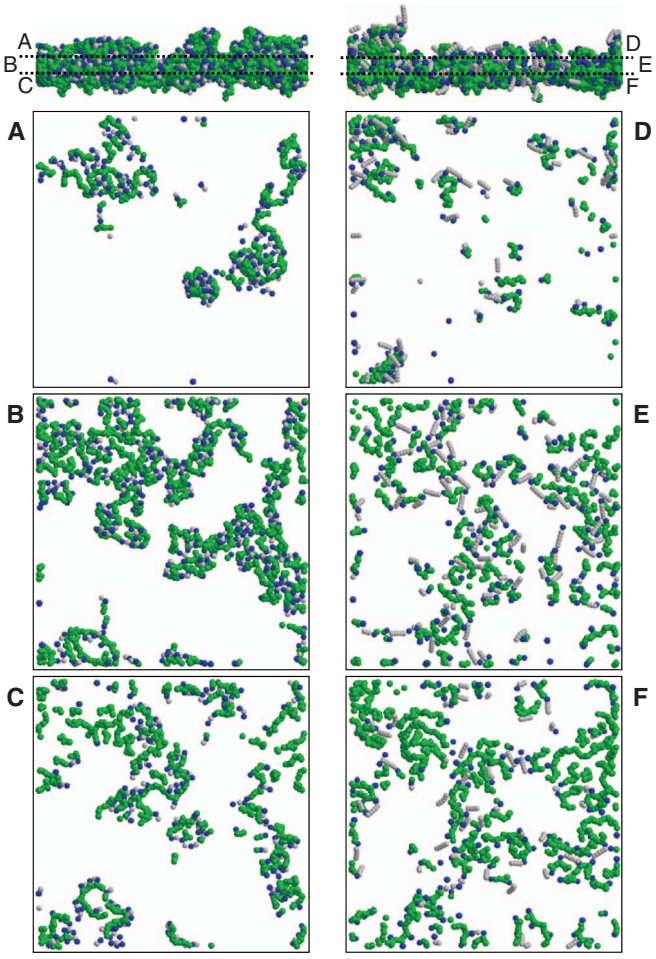

FIG. 6. yz side view of the entire porous structure and top-down views of three different cross-sectional slices of the dextran layers resulting from the immobilization of ligands employing type II counter-ions (A)–(C) and type VI counter-ions (D)–(F).

dextran chains have smaller densities and a higher degree of freedom. Below the interfacial regions are the interior bulk-like pore regions of the porous layers where, in comparison with the pore structure of the base dextran layer,[23] the numbers of smaller pores less than 20 Å in size can be seen to increase due to ligand immobilization at the cost of the intermediate in size pores in the size range of 30–50 Å, which essentially disappear in the bulk-like pore regions. This change is consistent with the conclusion from the comparison of the top-down views shown in Figure 3. Compared to type IV counter-ions, type III counter-ions having the same size and shape but half the valance, have been shown in Figures 2 and 3 to allow fewer ligands to be immobilized and a less compacted dextran layer, which is translated into more large in size pores in the outer interfacial region. Overall, type VI counter-ions appear to result in the lowest total number of pores in Figure 5, despite of the fact that they also allow the lowest number of ligands to be immobilized. This can be explained by the relatively large size and elongated shape of the counter-ions of type VI which require more physical pore space.

The pore connectivity of a porous medium is an important parameter that significantly affects the utilization of the pore volume and adsorption sites and, therefore, the effective mass transfer and adsorption rates of adsorbate biomolecules in the porous adsorbent medium.[4] From a statistical point of view, the level of pore connectivity of a porous medium can be assessed by the extent of crisscrossing between the spatial distribution curves in Figure 5 that represent pores of different size ranges along the direction z of net transport. A more detailed assessment of the connectivity between pores could be obtained by comparing lateral distributions of pores in consecutive cross sections at different depths. Figure 6 shows the pore structures and three consecutive cross sectional slices resulting from types II and VI counter-ions which, despite identical valance, result in the highest and the lowest ligand loadings, respectively, among the seven different types of counter-ions considered in this work. Starting from any point within the porous structures toward a new location, multiple pathways can be easily charted with or without going through more than one cross-sectional slice, which indicates good pore connectivities not only in the lateral directions but also in the perpendicular (net transport) direction. Furthermore, the effects of the size and shape of the counter-ions on ligand immobilization and pore structure can be seen to propagate down to great depths. The small spherical type II counter-ions are able to induce the immobilized ligands and

dextran segments to move close to each other to form local compact clusters. However, this tendency is diminished when the large elongated type VI counter-ions are used.

IV. CONCLUSIONS AND REMARKS

Molecular dynamics (MD) modeling and simulations have been performed in this work to study the effects of the counter-ions on the ligand immobilization process, the spatial distributions of the densities of the immobilized ligands and counter-ions, and the pore structure of the polymeric adsorbent medium. The results show that the porous adsorbent media formed by dextran polymer chains and immobilized ligand molecules are sensitive to the type of counter-ions present in the system and have mechanisms due to their structural steric resistances and covalent immobilization of charged ligands, which cause the charged ligands and the counter-ions to become unable to follow stoichiometric distributions so that local gradients in nonelectroneutrality and non-uniform density distributions of immobilized ligands are developed and, furthermore, exterior counter-ion clouds could be formed outside the porous layers. These phenomena can be reasoned from a fundamental point of view to be highly persistent during ligand immobilization for the construction of IEC porous polymeric adsorbent media and could also manifest themselves in systems with similar features. They can also be expected to affect very significantly the transport and adsorption mechanisms of adsorbate biomolecules when these porous adsorbent media are employed in bioseparations. The extent and magnitude of these counter-ion effects are found to depend on the sizes, shapes, structure, and charge of the counter-ions. The smallest spherical counter-ions have the least steric resistance to enter a porous structure and consequently result in small gradients in local nonelectroneutrality, higher ligand loadings and closer to uniform density distributions of immobilized ligands, and minimal formation of exterior counter-ion clouds. In contrast, counter-ions with significantly larger sizes and elongated shapes face substantially greater steric resistances to enter the porous structure and, thus, give rise to larger gradients in local nonelectroneutrality, lower ligand loadings and less uniform density distributions of immobilized ligands, and form significantly large in size exterior counter-ion clouds. The data of this work have indicated that the effects of lower counter-ion valence on the structure of the pore medium, the spatial density distribution and total number of immobilized ligands, and the formation of exterior counter-ion cloud are enhanced by the increased size and elongated structure of the counter-ion. From the results and discussion in this study, it would be physically unrealistic and practically undesirable to neglect the effects of the counter-ions on the formation of (i) a local gradient in nonelectroneutrality, (ii) a non-uniform spatial distribution of immobilized ligands, and (iii) a cloud of counter-ions located on the exterior of the porous dextran layer. These formations will influence the transport and adsorption rates of the adsorbate biomolecules when the polymeric porous adsorbent media are employed in chromatographic columns for effecting species separation by adsorption. Therefore, the MD modeling and simulation approach presented in this work could provide a means by which the effects of different counter-ions on ligand immobilization and on the pore structure of an adsorbent could be studied and, thus, contribute to the design and construction of polymeric porous adsorbent media that could provide high intraparticle mass transfer and adsorption rates that would result in high dynamic adsorption capacities for the desirable adsorbate biomolecules.

In practice, it could be probable that ionic impurities may exist which could influence the effects that the selected counter-ion has on the dynamics and equilibria of the ligand immobilization process. The MD modeling and simulation methodology of this work could be used and extended in order to determine the effects of possible ionic impurities on the behavior of the selected counter-ion and ligand, as well as on the pore structure during the ligand immobilization process.

[1]R. G. Harrison, P. Todd, S. R. Rudge, and D. R. Petrides, *Bioseperation Science and Engineering* (Oxford University Press, New York, 2003).
[2]C. F. Poole, *The Essence of Chromatography* (Elsevier, Amsterdam, 2003).
[3]A. I. Liapis and B. A. Grimes, J. Sep. Sci. **28**, 1909 (2005).
[4]E. Riccardi, J.-C. Wang, and A. I. Liapis, J. Chem. Phys. **133**, 084904 (2010).
[5]J.-C. Wang and A. I. Liapis, Chem. Ing. Tech. **83**, 152 (2011).
[6]H. Berg, H. Hansson, and L. Kagedal, "Adsorption/separation method and a medium for adsorption/separation," U.S. patent 6,428,707 B1 (6 August 2002).
[7]B.-L. Johansson, M. Belew, S. Eriksson, G. Glad, O. Lind, J.-L. Maloisel, and N. Norman, J. Chrmatogr. A **1016**, 21 (2003).
[8]B.-L. Johansson, M. Belew, S. Eriksson, G. Glad, O. Lind, J.-L. Maloisel, and N. Norman, J. Chrmatogr. A **1016**, 35 (2003).
[9]E. Riccardi, J.-C. Wang, and A. I. Liapis, J. Phys. Chem. B **112**, 7478 (2008).
[10]E. Riccardi, J.-C. Wang, and A. I. Liapis, J. Phys. Chem. B **113**, 2317 (2009).
[11]E. Riccardi, J.-C. Wang, and A. I. Liapis, J. Chromotogr. Sci. **47**, 459 (2009).
[12]A. I. Liapis, E. Riccardi, and J.-C. Wang, J. Sep. Sci. **33**, 2749 (2010).
[13]A. I. Liapis, Math. Model. Sci. Comput. **1**, 3 (1993).
[14]G. A. Heeter and A. I. Liapis, J. Chromatogr. A **743**, 3 (1996).
[15]J. J. Meyers and A. I. Liapis, J. Chromatogr. A **852**, 3 (1999).
[16]A. I. Liapis and B. A. Grimes, J. Sep. Sci. **30**, 648 (2007).
[17]J. C. Bosma and J. A. Wesselingh, AIChE J. **44**, 2399 (1998).
[18]J. A. Wesselingh and J. C. Bosma, AIChE J. **47**, 1571 (2001).
[19]M. Li and A. I. Liapis, J. Sep. Sci. **35**, 947 (2012).
[20]M. Li and A. I. Liapis, J. Sep. Sci. **36**, 1913 (2013).
[21]B. A. Grimes and A. I. Liapis, J. Colloid Interface Sci. **248**, 504 (2002).
[22]X. Zhang, B. A. Grimes, J.-C. Wang, K. M. Lacki, and A. I. Liapis, J. Colloid Interface Sci. **273**, 22 (2004).
[23]E. Riccardi, J.-C. Wang, and A. I. Liapis, J. Sep. Sci. **35**, 3073 (2012).
[24]C. James and J. Eastoe, Curr. Opin. Colloid Interface Sci. **18**, 40 (2013).
[25]H.-H. G. Tsai, W.-F. Juang, C.-M. Chang, T.-Y. Hou, and J.-B. Lee, Biochim. Biophys. Acta **1828**, 2729 (2013).
[26]B. M. Ladanyi, Curr. Opin. Colloid Interface Sci. **18**, 15 (2013).
[27]F. Rodriguez-Ropero and N. F. A. van der Vegt, Faraday Discuss. **160**, 297 (2013).
[28]F. A. Hamad, G. Chowdhury, and T. Matsuura, J. Membr. Sci. **191**, 71 (2001).
[29]A. V. Sangwai and R. Sureshkumar, Langmuir **28**, 1127 (2012).
[30]X. Zhang, J.-C. Wang, K. M. Lacki, and A. I. Liapis, J. Phys. Chem. B **109**, 21028 (2005).
[31]V. Molinero and W. A. Goddard, J. Phys. Chem. B **108**, 1414 (2004).
[32]M. P. Allen and D. J. Tildesley, *Computer Simulation of Liquids* (Clarendon Press, Oxford, 1987).
[33]D. Brown, and J. H. R. Clarke, Mol. Phys. **51**, 1243 (1984).
[34]J.-C. Wang and A. I. Liapis, J. Food. Eng. **110**, 514 (2012).